HHS Public Access

Author manuscript

Eur Radiol. Author manuscript; available in PMC 2018 November 01.

Published in final edited form as:

Eur Radiol. 2017 November ; 27(11): 4516–4524. doi:10.1007/s00330-017-4867-z.

Applying protein-based amide proton transfer MR imaging to distinguish solitary brain metastases from glioblastoma

Hao Yu[1], **Huiling Lou**[2], **Tianyu Zou**[1], **Xianlong Wang**[1], **Shanshan Jiang**[1,4], **Zhongqing Huang**[3], **Yongxing Du**[1], **Chunxiu Jiang**[1], **Ling Ma**[1], **Jianbin Zhu**[1], **Wen He**[1], **Qihong Rui**[1], **Jianyuan Zhou**[4], and **Zhibo Wen**[1]

[1]Department of Radiology, Zhujiang Hospital, Southern Medical University, Gongye Road M No. 253, Haizhu District, Guangzhou, Guangdong, 510282

[2]Department of Geriatrics, The First People' Hospital of Guangzhou, Guangzhou, Guangdong 510180, China

[3]Department of Medical Image Center, Yuebei People's Hospital, Shantou University Medical College, Shantou, Guangdong 515041, China

[4]Division of MR Research, Department of Radiology, Johns Hopkins University School of Medicine, 600N. Wolfe Street, Park 336, Baltimore, Maryland 21287, USA

Abstract

Objectives—To determine the utility of the amide proton transfer-weighted (APTw) MR imaging in distinguishing solitary brain metastases (SBMs) from glioblastomas (GBMs).

Methods—Forty-five patients with SBMs and forty-three patients with GBMs underwent conventional and APT-weighted sequences before clinical intervention. The APTw parameters and relative APTw (rAPTw) parameters in the tumor core and the peritumoral brain zone (PBZ) were obtained and compared between SBMs and GBMs. The receiver operating characteristic (ROC) curve was used to assess the best parameter for distinguishing between the two groups.

*Corresponding author: Please address correspondence to Zhibo Wen, MD. Professor Department of Radiology, Zhujiang Hospital, Southern Medical University, Gongye Road M No.253, Haizhu District, Guangzhou, Guangdong, 510282, China. Phone: +86-13802914951; 86-20-61643461. zhibowen@163.com.

Compliance with ethical standards:

Guarantor:

The scientific guarantor of this publication is Zhibo Wen M.D.

Conflict of interest:

The authors of this manuscript declare no relationships with any companies, whose products or services may be related to the subject matter of the article.

Statistics and biometry:

No complex statistical methods were necessary for this paper.

Informed consent:

Written informed consent was obtained from all subjects (patients) in this study.

Ethical approval:

Institutional Review Board approval was obtained.

Methodology:

- retrospective
- diagnostic or prognostic study
- performed at one institution

Results—The $APTw_{max}$, $APTw_{min}$, $APTw_{mean}$, $rAPTw_{max}$, $rAPTw_{min}$ or $rAPTw_{mean}$ values in the tumor core were not significantly different between the SBM and GBM groups (*P*=0.141, 0.361, 0.221, 0.305, 0.578 and 0.448, respectively). However, the $APTw_{max}$, $APTw_{min}$, $APTw_{mean}$, $rAPTw_{max}$, $rAPTw_{min}$ or $rAPTw_{mean}$ values in the PBZ were significantly lower in the SBM group than in the GBM group (P<0.001). The $APTw_{min}$ values had the highest area under the ROC curve 0.905 and accuracy 85.2% in discriminating between the two neoplasms.

Conclusion—As a noninvasive imaging method, APT-weighted MR imaging can be used to distinguish SBMs from GBMs.

Keywords

glioblastoma; solitary brain metastases; APT imaging; brain; magnetic resonance imaging

Introduction

According to the West China Glioma Center (WCGC) and Central Brain Tumor Registry of the United States (CBTRUS), metastasis and glioma are the most frequent malignant brain neoplasms, and the incidence rate of both diseases has been increasing in recent decades [1; 2]. The ability to distinguish metastases from glioma is critical because the therapeutic planning and follow-up of these tumors are vastly different [3]. If metastasis is suspected, high-dose Gd should be used to elucidate other metastases in the brain [4], and other parts of the body should be examined. For metastasis therapy, nonsurgical treatment is preferred over conventional surgical resection [5]. However, when glioma is suspected, various advanced MRI techniques are required to detect the true tumor margin, and surgical resection is the first choice [6]. Usually, differentiation between the two neoplasms depends primarily on clinical history, particularly in cases with multiple lesions. However, if the patient's clinical history is uncertain, or the lesion is solitary, the distinction of these neoplasms may be difficult [7]. On conventional MRI, there is substantial overlap between the images of solitary brain metastases (SBMs) and glioblastomas (GBMs), as both manifest similar signal features and contrast enhancement patterns. Previously, investigators worldwide use DWI, PWI, MRS, and ASL perfusion imaging to differentiate between these tumors [8–11]. However, the distinction between these two types of tumors still has limited diagnostic specificity.

Amide proton transfer-weighted (APTw) MR imaging was invented by Zhou and van Zijl et al. and is a novel molecular MRI technique based on chemical exchange-based saturation transfer (CEST), which was designed to detect amide protons of endogenous low-concentration mobile proteins and peptides in tissue [12–14]. This technique does not require the use of exogenous contrast agents and is applied to imaging through the exchange between amide protons of mobile proteins and peptides and protons of bulk water. The APTw signals are mainly related to cell density and endogenous mobile proteins and peptides [15–18]. APTw imaging has emerged as a valuable tool for grading brain tumors[18–20] and other cancers that occur in the prostate [21], breast [22; 23] and neck [24; 25]; for distinguishing tumor recurrence from radiation necrosis [26], distinguishing pseudo-progression from true progression in gliomas [27], and differentiating between primary central nervous system lymphomas and glioma [15]; and for characterizing cerebral

ischemia [28–30]and Parkinson's disease [31]. However, this technique has not been used to compare SBMs and GBMs. Therefore, the purpose of this study was to evaluate the usefulness of APTw MRI in distinguishing SBMs from GBMs at the molecular level based on their APTw values.

Materials and Methods

Study population

The institutional review board of our hospital approved this study, and each patient signed the consent form. From May 2011 to October 2016, ninety-four patients with SBMs or GBMs were recruited and received conventional and APTw MRI. Data from six patients were excluded because of insufficient image quality due to motion artefacts. Therefore, eighty-eight patients were included in this study. Forty-five patients (thirty-three males, twelve females; age range, 30–74 years; mean age, 56.5±9.2 years) had SBMs were confirmed by histopathology(n=39) or clinical diagnosis(n=6), the primary sites of cancers included lung (n=28), breast (n=6), kidney (n=4), colon (n=4), liver (n=2), and the lymphatic system (n=1); and forty-three patients (twenty-nine males, fourteen females; age range, 18–71 years; mean age, 44.8±13.8 years) had GBMs confirmed by histopathology.

MR imaging

All patients underwent a conventional brain MRI sequence and two-dimensional (2D) APTw sequence on a 3.0 T MRI scanner (Achieva 3.0 T; Philips Medical Systems, Best, The Netherlands) before clinical intervention. A body coil was used for radiofrequency (RF) transmission, and a 16-channel head coil was used for signal reception. Conventional MRI sequences included T_1-weighted (repetition time (ms)/echo time (ms), 400/20), T_2-weighted (repetition time (ms)/echo time (ms), 2800/105), fluid-attenuated inversion recovery (FLAIR, repetition time (ms)/echo time (ms)/inversion recovery time (ms) 8000/204/2200). Then, a contrast agent (Gd-DTPA; 0.2 ml/kg body weight; Magnevist; Bayer Schering, Guangzhou, China) was injected through the median cubital vein, and gadolinium-enhanced T_1-weighted images were acquired. Other imaging parameters were as follows: field of view, 240×240 mm^2; slice thickness, 5 mm; gap, 2 mm; matrix, 512×512.

The 2D fat-suppressed, fast spin-echo APTw pulse sequence was performed at one T_2-weighted image slice showing the maximum area of the tumor before Gd-T_1-weighted image. For saturation, a pulse-train radiofrequency saturation (duration time=800 ms; inter-pulse delay=10 ms; power level=2 μT) was used. APTw imaging was performed with a multi-offset (offsets=0, ±0.25, ±0.5, ±0.75, ±1, ±1.5, ±2, ±2.5, ±3, ±3.25, ±3.5, ±3.75, ±4, ±4.5, ±5 and ±6 ppm) multi-acquisition protocol. The protocol was repeated 8 times at an offset of ±3.5 ppm to increase the signal-to-noise ratio of the APTw images. In addition, an image that did not exert a saturated pulse was acquired for the signal normalization, and an image that exerted a saturated pulse at the offset of 15.6 ppm was acquired to calculate the conventional MTR value. The detailed imaging parameters were as follows: sensitivity-encoding factor = 2, repetition time (s), 3; echo time (ms), 11; field of view, 240×240 mm^2; section thickness, 6 mm; matrix, 128×128; voxel size, 1.65×3.15×6.00 mm^3. The total acquisition time was 192 seconds.

Image analysis

The APTw raw data were analyzed using interactive data language written in the program (IDL; Research Systems, Inc., Boulder, CO, USA). First, the normalized saturated signal intensity curve (S_{sat}/S_0, where S_{sat} and S_0 were the signal intensities obtained with and without selective saturation, respectively) as a function of saturation frequency offset, usually called the Z-spectrum, was calculated. B_0 field inhomogeneity effect was corrected, as described previously [18]. To reduce the contributions from conventional magnetization transfer contrast and direct saturation of bulk water, a B_0-corrected Z-spectrum was used to analyze the magnetization transfer ratio asymmetry (MTR_{asym}) as follows: $MTR_{asym}=S_{sat}(-offset)/S_0-S_{sat}(+offset)/S_0$. The APTw signal was calculated as $MTR_{asym}(3.5ppm)$.

Images analysis was performed by two experienced neuroradiologists (L.W. and S.J., who have 11 and 10 years of experience in neuroradiology, respectively). Tumor enhancement type and edema index (EI) was recorded; Five regions of interest (ROIs) were distributed within the Gd-enhancing tumor area, as well as within the peritumoral brain zone (PBZ; peritumoral T_2w hyperintense area, 0.5–2.5 cm from the enhancing tumor area to avoid partial volume contamination) (Fig. 1), based on the Gd-T_1WI and T_2WI co-registered with the APTw image [32]. Large cystic cavities and hemorrhagic components were always excluded. The size of each ROI was 15 pixels. In addition, the contralateral normal-appearing white matter (CNAWM) was analyzed (Fig. 1). For each patient, the APTw values for all ROIs were recorded. Then, the maximum APTw value ($APTw_{max}$), minimum APTw value ($APTw_{min}$) and mean APTw value ($APTw_{mean}$) were determined. To reduce the effect of patient age [33] and other potential experimental errors[34], we also recorded relative APTw (rAPTw = APTw - $APTw_{CNAWM}$): $rAPTw_{max}$, $rAPTw_{min}$ and $rAPTw_{mean}$.

Pathological data acquisition

The pathologic images were analyzed with image analysis software (Image-Pro Plus, version 6.0, Media Cybernetics, Silver Spring, MD, USA). One neuropathologist, blinded to the MRI features, reviewed the hematoxylin and eosin (H&E)-stained biopsy samples from the tumor core and the PBZ of 39 patients with SBM and 43 patients with GBM. The pathological type and tumor grade were recorded according to 2007 WHO classification of tumors of the CNS. The presence of infiltrating cells in the PBZ was also estimated.

Statistical analysis

Statistical analysis performed was statistical analysis software packages (SPSS19.0 and MedCalc v13.1.2.0). The patient's gender was comparedbetween SBMs and GBMs using the Chi-square test, Comparison among $APTw_{mean}$ values for the tumor core, PBZ and CNAWM were performed using a one-way analysis of variance (ANOVA) test, followed by multiple comparisons using Tukey test, to analyze the statistical significance of differences. Comparison between patient's age, $APTw_{CNAWM}$, $APTw_{max}$, $APTw_{min}$, $APTw_{mean}$, $rAPTw_{max}$, $rAPTw_{min}$, or $rAPTw_{mean}$ values for SBMs and GBMs were performed using an independent-samples *t*-test. Receiver operating characteristic (ROC) curves were generated for each parameter to assess the areas under the curves (AUCs) and to determine optimal

cut-off values according to Youden's index for the discrimination of SBMs and GBMs. *P*<0.05 was considered a statistically significant difference for all tests.

Results

There was no gender difference between the SBMs and GBMs groups (*P=0.545*). The patients age was higher in the SBM group than the GBM patients (*P*<0.001).

Pathological data

In biopsy samples from PBZ, the tumor cells were presence in 29/43 samples; by contrast, 7/39 samples were presence in the SBM group.

Comparison of conventional and APTw image features

For 45 cases of SBMs (45 lesions) were located in the cerebral parenchyma (n=36) and in the cerebellar hemisphere (n=9). 8 cases showed mild edema, 26 cases showed moderate edema, and 11 cases showed severe edema. On the Gd-T_1WI, tumors showed ring-like (n=13), nodular (n=22) or patchy (n=10) enhancement. The tumors cores showed hyperintensities (relative to the CNAWM) on the APTw images, and the hyperintense areas on APTw images were approximately equal to the lesions shown on the Gd-T_1WI. For the 43 cases of GBMs (43 lesions), the lesions were located in the cerebral parenchyma (n=35) brainstem (n=2) and in the cerebellar hemisphere (n=6). 7 cases showed mild edema, 30 cases showed moderate edema, and 6 cases showed severe edema. In the Gd-T_1WI, the tumors showed ring-like (n=24), nodular (n=11) or patchy (n=8) enhancement. Compared with the CNAWM, the lesions identified by the APTw image were larger than those identified by the Gd-T_1WI. Fig. 2 shows a SBM patient, and Fig. 3 shows a GBM patient.

Quantitative APTw image analysis

The APTw value in the CNAWM was significantly lower in SBMs than in GBMs (0.49% ±0.18% vs. 0.54%±0.14%, *P*=0.046). The APTw value in the tumor core of SBMs and GBMs was significantly higher than in the CNAWM (2.76%±0.71% vs. 0.49%±0.18%, P<0.001 and 2.94%±0.67% vs. 0.54%±0.14%, P<0.001). The $APTw_{mean}$ in the PBZ of SBMs and GBMs was significantly higher than in the CNAWM (1.23%±0.23% vs. 0.49% ±0.18%, P<0.001 and 1.71%±0.34% vs. 0.54%±0.14%, P<0.001). The $APTw_{max}$, $APTw_{min}$, $APTw_{mean}$, $rAPTw_{max}$, $rAPTw_{min}$ or $rAPTw_{mean}$ in the tumor core showed significant differences between SBMs and GBMs (P>0.05). By contrast, all parameters in the PBZ were lower in the SBMs than in the GBMs (P<0.001) (Table 1 and Fig. 4).

ROC analyses of the APTw parameters values in the PBZ are summarized in Table 2. The $APTw_{min}$ had the highest AUC of 0.905. When the $APTw_{min}$ of the PBZ was less than 1.21%, the lesion was diagnosed as an SBM. The sensitivity was 84.4%, the specificity was 86.1% and the accuracy was 85.2% (Table 2).

Discussion

In this study, the gender distribution of patients with SBMs was not show significantly different from that of patients with GBMs, although these two tumor types have been shown

to be more common in males. Tan et al. [35] found that there was no age difference between SBM group and high-grade glioma group, but our result shows the SBM patients were significantly older than the GBM patients. As in a previous study [33; 34], the white matter volume was observed to decline after 50 years of age due to demyelination, and the APTw effect due to the myelin basic protein shifted from the oligodendroglia cytoplasm to the myelin sheath. Therefore, we speculated that this was the reason that the APTw parameter value of the CNAWM was lower in the SBM group.

Whether the tumor core can be reliably discriminated between SBMs and GBMs with conventional MRI, even with several advanced MRI techniques such as DWI, PWI, MRS, DTI and ASL, is still have controversial [3; 8; 11; 35–37]. Previous studies have shown that APTw MRI can identify the tumor core mainly related to mobile amide proton content and cell density, which was not relevant to Gd enhancement [16; 18]. This finding is particularly important in the context of grade glioma, because 10% of patients with glioblastoma may demonstrate non-enhancement on Gd-T_1WI [15], which may avoid central nervous system damage and nephrogenic systemic fibrosis caused by Gd deposition during reexamination [38; 39]. Here we use APTw imaging to distinguish between SBMs and GBMs. Compared with the CNAWM, both SBMs and GBMs, exhibited tumor core shown hyperintensity on APTw images. Quantitative $APTw_{min}$, $APTw_{max}$, $APTw_{mean}$, $rAPTw_{min}$, $rAPTw_{max}$ or $rAPTw_{mean}$ values of the tumor core were not significantly different ($P>0.05$). It is well known that as malignant tumors SBMs and GBMs exhibit rapid cell proliferation in the tumor core [35], and that the cell density and mobile proteins and peptides are higher than that of the CNAWM. However, the difference in proton content between SBMs and GBMs is expected to be negligible. An investigation of the tumor core using APTw MRI cannot provide useful information to distinguishing SBMs from GBMs.

The peritumoral brain zone (PBZ) is defined radiologically as the non-enhancing brain area of several centimeters in width surrounding the tumor in Gd-T_1WI. Usually, this area shows hyper-intensity on T_2WI and FLAIR images due to vasogenic edema [40]; as the blood-brain barrier breaks down, capillary permeability increases, a pressure gradient from the vasculature to the extracellular environment is formed, and many intravascular proteins penetrate into the extra-cellular space [41]. In this study, the APTw value in the PBZ of SBMs and GBMs was significantly higher than in the CNAWM ($P<0.001$). It is interesting to note that the values of $APTw_{min}$, $APTw_{max}$, $APTw_{mean}$, $rAPTw_{min}$, $rAPTw_{max}$ or $rAPTw_{mean}$ in the SBM group were significantly lower than in the GBM group ($P<0.001$). In metastases brain tumors, PBZ T_2 hyperintensity mainly reflects vasogenic edema [7; 35]. In the GBMs, it is hypothesized that specific cells and inflammatory cells infiltrate into the PBZ [40; 42–44], and that the PBZ T_2 hyperintensity reflects more than vasogenic edema. Technically, the APTw effect is due to the shift of amide proton from mobile proteins and peptides to water proton [12]. In the PBZ of GBMs, other than intravascular proteins, because of the infiltration of tumor cells and inflammatory cells, the tumor-related molecules and inflammatory mediators are also retained in the extra-cellular space of the PBZ [41; 45], and the mobile protein and peptide content may be higher than in SBMs. The pathological examination of PBZ supports this hypothesis. Notably, the APTw value in the PBZ of SBMs was significantly higher than in the CNAWM. We speculate that, as the

intravascular proteins penetrate into the extra-cellular space of the PBZ, the amide proton content exceeds that in the CNAWM [41].

According to ROC curve analysis, the $APTw_{min}$ had the highest AUC (0.905) and accuracy (85.2%) for distinguishing between SBMs and HGGs. For the 88 participants in this study, the accuracy for differentiating SBMs from GBMs was 51.6% (by Y.D., a junior radiologist with 3 years of experience in brain imaging, blinded to the pathology reports, based on conventional MRI sequences) and 79.5% (according to official radiology reports, performed by senior neuro-radiologists in our department). Compared with conventional MRI, protein-based APT_W imaging can improve the accuracy for discriminating between SBMs and GBMs.

On conventional MRI images, although glioma cells infiltrate into the PBZ, the blood-brain barrier does not break down, and enhancement is not observed in Gd-T_1WI [18]. However, the cell density and mobile proteins and peptides in the PBZ have increased; in the PBZ of GBMs, the APTw value was higher closer to the tumor core than the APTw value in the CNAWM; thus, the APTw MRI, which is based on amide protons, may provide new insights into the evaluation the extrent of GBM cell infiltration in the PBZ on a molecular level.

However, this study has several limitations. First, the sample size of the metastases group is mainly involving the metastasis of lung cancer. A larger sample size that includes metastases of more primary cancers is required for more reliable results. Second, the APT-weighted sequence covered only one slice, and the MRI signal changes in other tumor regions could not be evaluated in the present study. Third, in the current study, the voxel size of the APT-weighted sequence was relatively large (due to the small APT effect), which may have led to homogeneous APTw hyperintensities due to the large partial volume effect.

In conclusion, APT-weighted MRI can differentiate between solitary brain metastases and glioblastoma, which indicates that comparisons in APTw parameters in the peritumoral edema may be useful for differentiating between SBMs and GBMs. The $APTw_{min}$ has the highest sensitivity, specificity and accuracy. As a safe and completely non-invasive imaging technique, APT-weighted MRI could be a supplement to improve the preoperative diagnosis of SBMs and GBMs in the clinic.

Acknowledgments

This study was partially supported by grants from National Natural Science Foundation of China (81171322), Guangdong Provincial Natural Science Foundation (2014A030313271, S2012010009114), Guangdong Provincial Science and Technology Project (2014A020212726), Southern Medical University clinical research project (LC2016ZD028), and the National Institutes of Health (R01EB009731, R01CA166171).

Funding:

This study is partially supported by grants from National Natural Science Foundation of China (81171322), Natural Science Foundation of Guangdong Province (2014A030313271), Guangdong Provincial Science and Technology Project (2014A020212726), Natural Science Foundation of Guangdong Province (S2012010009114), Southern Medical University clinical research project (LC2016ZD028) and the National Institutes of Health (R01EB009731, R01CA166171).

Abbreviations

GBM	glioblastoma
SBM	solitary brain metastases
APT	amide proton transfer
APTw	APT-weighted
rAPTw	relative APTw
CEST	chemical exchange-based saturation transfer
CNAWM	contralateral normal-appearing white matter
Gd	gadolinium
H&E	hematoxylin and eosin
PBZ	peritumoral brain zone

References

1. Wang X, Chen JX, Zhou Q, et al. Statistical Report of Central Nervous System Tumors Histologically Diagnosed in the Sichuan Province of China from 2008 to 2013: A West China Glioma Center Report. Annals of surgical oncology. 2016; doi: 10.1245/s10434-016-5410-1
2. Ostrom QT, Gittleman H, Fulop J, et al. CBTRUS Statistical Report: Primary Brain and Central Nervous System Tumors Diagnosed in the United States in 2008–2012. Neuro-oncology. 2015; 17(Suppl 4):iv1–iv62. [PubMed: 26511214]
3. Blanchet L, Krooshof PW, Postma GJ, et al. Discrimination between metastasis and glioblastoma multiforme based on morphometric analysis of MR images. AJNR American journal of neuroradiology. 2011; 32:67–73. [PubMed: 21051512]
4. Yuh WT, Engelken JD, Muhonen MG, Mayr NA, Fisher DJ, Ehrhardt JC. Experience with high-dose gadolinium MR imaging in the evaluation of brain metastases. AJNR American journal of neuroradiology. 1992; 13:335–345. [PubMed: 1595472]
5. Owonikoko TK, Arbiser J, Zelnak A, et al. Current approaches to the treatment of metastatic brain tumours. Nature reviews Clinical oncology. 2014; 11:203–222.
6. Wen PY, Kesari S. Malignant gliomas in adults. The New England journal of medicine. 2008; 359:492–507. [PubMed: 18669428]
7. Lee EJ, Ahn KJ, Lee EK, Lee YS, Kim DB. Potential role of advanced MRI techniques for the peritumoural region in differentiating glioblastoma multiforme and solitary metastatic lesions. Clinical radiology. 2013; 68:e689–697. [PubMed: 23969153]
8. Han CK, Huang SM, Guo JF, Zhuang XJ, Han HW. Use of a high b-value for diffusion weighted imaging of peritumoral regions to differentiate high-grade gliomas and solitary metastases. J Magn Reson Imaging. 2015; 42:80–86. [PubMed: 25223489]
9. Abe T, Mizobuchi Y, Sako W, et al. Clinical Significance of Discrepancy between Arterial Spin Labeling Images and Contrast-enhanced Images in the Diagnosis of Brain Tumors. Magn Reson Med Sci. 2015; 14:313–319. [PubMed: 26104074]
10. Caivano R, Lotumolo A, Rabasco P, et al. 3 Tesla magnetic resonance spectroscopy: cerebral gliomas vs. metastatic brain tumors. Our experience and review of the literature. Int J Neurosci. 2013; 123:537–543. [PubMed: 23390934]
11. Mouthuy N, Cosnard G, Abarca-Quinones J, Michoux N. Multiparametric magnetic resonance imaging to differentiate high-grade gliomas and brain metastases. Journal of neuroradiology Journal de neuroradiologie. 2012; 39:301–307. [PubMed: 22197404]

12. Zhou J, Lal B, Wilson DA, Laterra J, van Zijl PC. Amide proton transfer (APT) contrast for imaging of brain tumors. Magn Reson Med. 2003; 50:1120–1126. [PubMed: 14648559]
13. Zhou J, Payen JF, Wilson DA, Traystman RJ, van Zijl PC. Using the amide proton signals of intracellular proteins and peptides to detect pH effects in MRI. Nature medicine. 2003; 9:1085–1090.
14. van Zijl PCM, Yadav NN. Chemical Exchange Saturation Transfer (CEST): What is in a Name and What Isn't? Magn Reson Med. 2011; 65:927–948. [PubMed: 21337419]
15. Jiang SS, Yu H, Wang XL, et al. Molecular MRI differentiation between primary central nervous system lymphomas and high-grade gliomas using endogenous protein-based amide proton transfer MR imaging at 3 Tesla. Eur Radiol. 2016; 26:64–71. [PubMed: 25925361]
16. Zhou J, Zhu H, Lim M, et al. Three-dimensional amide proton transfer MR imaging of gliomas: Initial experience and comparison with gadolinium enhancement. J Magn Reson Imaging. 2013; 38:1119–1128. [PubMed: 23440878]
17. Togao O, Kessinger CW, Huang G, et al. Characterization of Lung Cancer by Amide Proton Transfer (APT) Imaging: An In-Vivo Study in an Orthotopic Mouse Model. Plos One. 2013:8.
18. Wen ZB, Hu SG, Huang FH, et al. MR imaging of high-grade brain tumors using endogenous protein and peptide-based contrast. Neuroimage. 2010; 51:616–622. [PubMed: 20188197]
19. Togao O, Hiwatashi A, Yamashita K, et al. Grading diffuse gliomas without intense contrast enhancement by amide proton transfer MR imaging: comparisons with diffusion- and perfusion-weighted imaging. Eur Radiol. 2016; doi: 10.1007/s00330-016-4328-0:1-11
20. Sakata A, Okada T, Yamamoto A, et al. Grading glial tumors with amide proton transfer MR imaging: different analytical approaches. Journal of neuro-oncology. 2015; 122:339–348. [PubMed: 25559689]
21. Jia G, Abaza R, Williams JD, et al. Amide proton transfer MR imaging of prostate cancer: a preliminary study. J Magn Reson Imaging. 2011; 33:647–654. [PubMed: 21563248]
22. Klomp DWJ, Dula AN, Arlinghaus LR, et al. Amide proton transfer imaging of the human breast at 7T: development and reproducibility. Nmr Biomed. 2013; 26:1271–1277. [PubMed: 23559550]
23. Dula AN, Arlinghaus LR, Dortch RD, et al. Amide proton transfer imaging of the breast at 3 T: Establishing reproducibility and possible feasibility assessing chemotherapy response. Magn Reson Med. 2013; 70:216–224. [PubMed: 22907893]
24. Wang J, Weygand J, Hwang KP, et al. Magnetic Resonance Imaging of Glucose Uptake and Metabolism in Patients with Head and Neck Cancer. Scientific reports. 2016; 6:30618. [PubMed: 27461165]
25. Yuan J, Chen S, King AD, et al. Amide proton transfer-weighted imaging of the head and neck at 3 T: a feasibility study on healthy human subjects and patients with head and neck cancer. Nmr Biomed. 2014; 27:1239–1247. [PubMed: 25137521]
26. Zhou JY, Tryggestad E, Wen ZB, et al. Differentiation between glioma and radiation necrosis using molecular magnetic resonance imaging of endogenous proteins and peptides. Nature medicine. 2011; 17:130–U308.
27. Ma B, Blakeley JO, Hong X, et al. Applying amide proton transfer-weighted MRI to distinguish pseudoprogression from true progression in malignant gliomas. J Magn Reson Imaging. 2016; 44:456–462. [PubMed: 26788865]
28. Tietze A, Blicher J, Mikkelsen IK, et al. Assessment of ischemic penumbra in patients with hyperacute stroke using amide proton transfer (APT) chemical exchange saturation transfer (CEST) MRI. Nmr Biomed. 2014; 27:163–174. [PubMed: 24288260]
29. Tee YK, Harston GWJ, Blockley N, et al. Comparing different analysis methods for quantifying the MRI amide proton transfer (APT) effect in hyperacute stroke patients. Nmr Biomed. 2014; 27:1019–1029. [PubMed: 24913989]
30. Zhao XN, Wen ZB, Huang FH, et al. Saturation Power Dependence of Amide Proton Transfer Image Contrasts in Human Brain Tumors and Strokes at 3 T. Magn Reson Med. 2011; 66:1033–1041. [PubMed: 21394783]
31. Li CM, Peng S, Wang R, et al. Chemical exchange saturation transfer MR imaging of Parkinson's disease at 3 Tesla. Eur Radiol. 2014; 24:2631–2639. [PubMed: 25038850]

32. Zhang Y, Heo HY, Lee DH, et al. Selecting the reference image for registration of CEST series. J Magn Reson Imaging. 2016; 43:756–761. [PubMed: 26268435]
33. Zhang H, Kang H, Zhao X, et al. Amide Proton Transfer (APT) MR imaging and Magnetization Transfer (MT) MR imaging of pediatric brain development. Eur Radiol. 2016; 26:3368–3376. [PubMed: 26762941]
34. Allen JS, Bruss J, Brown CK, Damasio H. Normal neuroanatomical variation due to age: The major lobes and a parcellation of the temporal region. Neurobiol Aging. 2005; 26:1245–1260. [PubMed: 16046030]
35. Tan Y, Wang XC, Zhang H, et al. Differentiation of high-grade-astrocytomas from solitary-brain-metastases: Comparing diffusion kurtosis imaging and diffusion tensor imaging. European journal of radiology. 2015; 84:2618–2624. [PubMed: 26482747]
36. Crisi G, Orsingher L, Filice S. Lipid and macromolecules quantitation in differentiating glioblastoma from solitary metastasis: a short-echo time single-voxel magnetic resonance spectroscopy study at 3 T. Journal of computer assisted tomography. 2013; 37:265–271. [PubMed: 23493217]
37. Lee EJ, terBrugge K, Mikulis D, et al. Diagnostic value of peritumoral minimum apparent diffusion coefficient for differentiation of glioblastoma multiforme from solitary metastatic lesions. AJR American journal of roentgenology. 2011; 196:71–76. [PubMed: 21178049]
38. Ramalho J, Castillo M, AlObaidy M, et al. High Signal Intensity in Globus Pallidus and Dentate Nucleus on Unenhanced T1-weighted MR Images: Evaluation of Two Linear Gadolinium-based Contrast Agents. Radiology. 2015; 276:836–844. [PubMed: 26079490]
39. Collidge TA, Thomson PC, Mark PB, et al. Gadolinium-enhanced MR imaging and nephrogenic systemic fibrosis: retrospective study of a renal replacement therapy cohort. Radiology. 2007; 245:168–175. [PubMed: 17704357]
40. Lemee JM, Clavreul A, Aubry M, et al. Characterizing the peritumoral brain zone in glioblastoma: a multidisciplinary analysis. Journal of neuro-oncology. 2015; 122:53–61. [PubMed: 25559687]
41. Oh J, Cha S, Aiken AH, et al. Quantitative apparent diffusion coefficients and T2 relaxation times in characterizing contrast enhancing brain tumors and regions of peritumoral edema. J Magn Reson Imaging. 2005; 21:701–708. [PubMed: 15906339]
42. Goplen D, Bougnaud S, Rajcevic U, et al. alpha B-Crystallin Is Elevated in Highly Infiltrative Apoptosis-Resistant Glioblastoma Cells. Am J Pathol. 2010; 177:1618–1628. [PubMed: 20813964]
43. Parney IF, Waldron JS, Parsa AT. Flow cytometry and in vitro analysis of human glioma-associated macrophages. Laboratory investigation. Journal of neurosurgery. 2009; 110:572–582. [PubMed: 19199469]
44. Frieboes HB, Zheng X, Sun CH, Tromberg B, Gatenby R, Cristini V. An integrated computational/experimental model of tumor invasion. Cancer research. 2006; 66:1597–1604. [PubMed: 16452218]
45. Fazi B, Felsani A, Grassi L, et al. The transcriptome and miRNome profiling of glioblastoma tissues and peritumoral regions highlights molecular pathways shared by tumors and surrounding areas and reveals differences between short-term and long-term survivors. Oncotarget. 2015; 6:22526–22552. [PubMed: 26188123]

Key Points

- APTw values in the tumor core were not different between SBMs and GBMs.
- APTw values in the peritumoral brain zone were lower in SBMs than in GBMs.
- The $APTw_{min}$ was the best parameter to distinguish SBMs from GBMs.

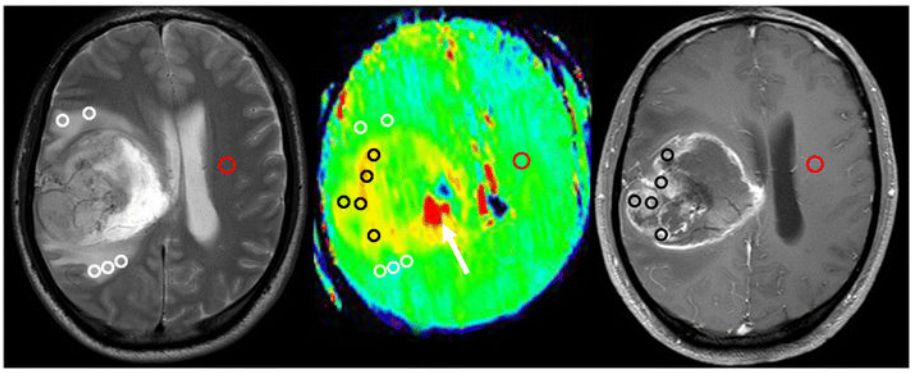

Fig. 1.

Example of the placement of ROIs. Five ROIs were placed in the Gd-enhancing tumor part (Black Circle), five ROIs were placed in the peritumoral T_2 hyper-intensity area (White Circle), and one ROI was placed in the contralateral normal-appearing white matter (Red Circle) based on the co-registered traditional images. The necrosis-related image artefact (white arrow) can also be seen.

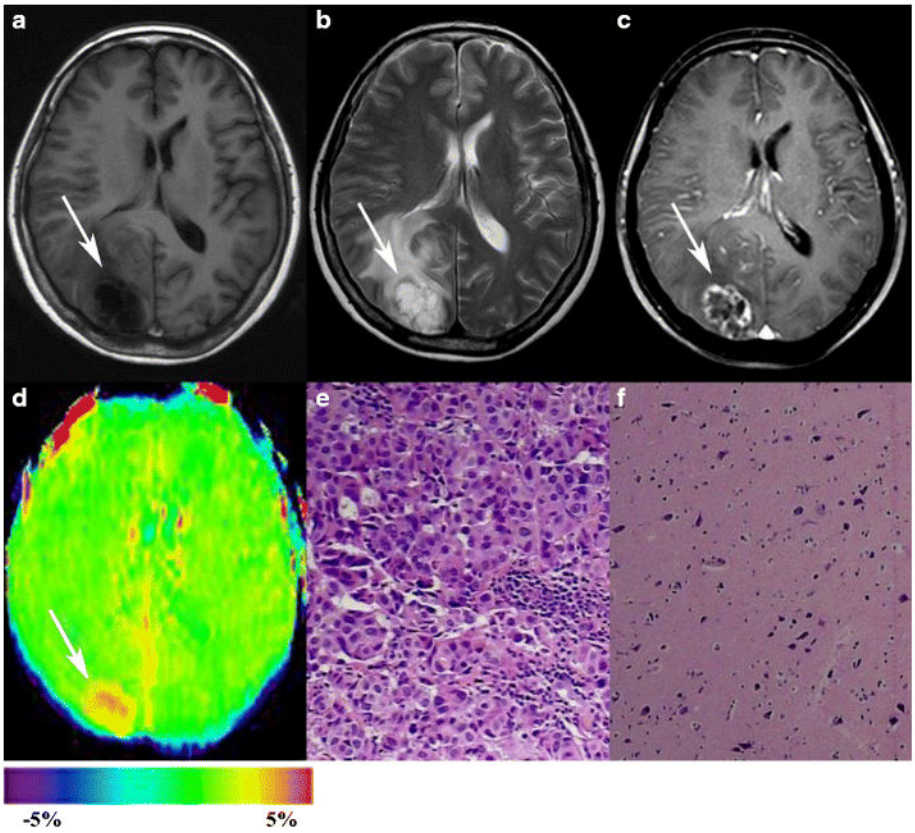

Fig. 2.

Results for a 54-year-old woman with solitary brain metastasis (white arrows). The primary tumor was lung adenocarcinoma. A–C, the tumor was located in the right parietal-occipital lobe with moderate peritumoral edema. It appears hypointense on T_1WI, hyperintense on T_2WI, and ring-like contrast-enhanced on Gd-T_1WI. D, an APTw image shows a relatively homogeneous hyperintense mass (tumor core, APT_{Wmax}=3.55%, APT_{Wmin}=2.87%, APT_{Wmean}=3.34%; peritumoral edema, APT_{Wmax}=1.72%, APT_{Wmin}=1.57%, APT_{Wmean}=1.63%; APT_{WCNAWM}= 0.74%). E, H&E-stained sections (×200) of the tumor core show many dense, aggregated cells with atypical nuclei arranged in glandular, nest and cord patterns. F, H&E-stained sections (×100) of the peritumoral edema show the degeneration of nerve cells and the proliferation of glial cells, but no tumor cells are found.

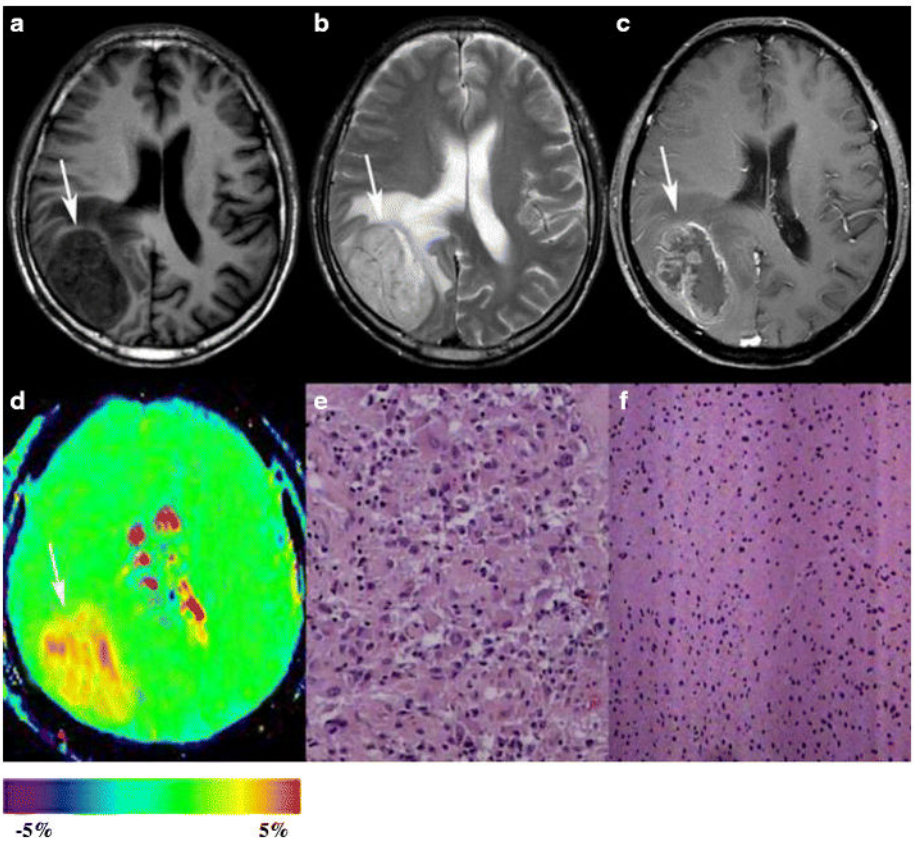

Fig. 3.

Results for a 67-year-old man with glioblastoma. A–C, the tumor is located in the right occipital lobe with mild peritumoral edema. The tumor appears hypointense on the T_1WI, hyperintense on the T_2WI, and ring-like contrast-enhanced on the Gd-T_1WI. D, an APT_W image shows a heterogeneously hyperintense mass (tumor core: APT_{Wmax}=3.87%, APT_{Wmin}=2.96%, $APT_{Wmean=}$3.61%; peritumoral edema: APT_{Wmax}=2.09%, APT_{Wmin}=1.63%, APT_{Wmean}=1.89%; APT_{WCNAWM} =0.57%). E, H&E-stained sections (×200) of the tumor core show many multinucleated atypical tumor cells with relatively abundant cytoplasm. F, H&E-stained sections (×100) of the peritumoral edema show proliferating glial cells and a number of cells with atypical nuclei.

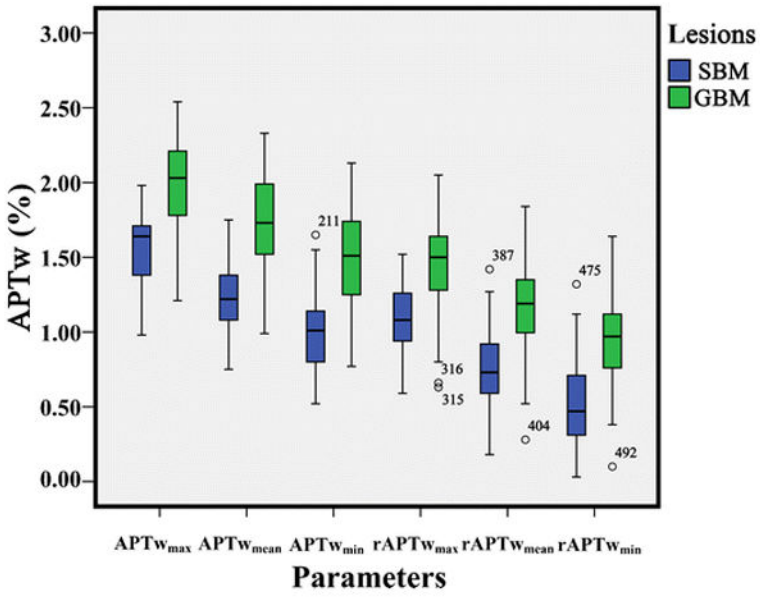

Fig. 4.

Box-and-whisker plots. Thick horizontal line=mean, whiskers=±SD. APTw values in the SBM group are significantly lower than those in the GBM group (all $P < 0.001$).

Table 1

APT_W parameter values of the tumor core and peritumoral brain zone

Parameter	Tumor core		P	Peritumoral brain zone		P
	SBM	GBM		SBM	GBM	
$APTw_{max}$	2.98%±0.74%	3.22%±0.75%	0.141	1.56%±0.22%	1.98%±0.31%	<0.001
$APTw_{min}$	2.53%±0.70%	2.66%±0.63%	0.361	0.98%±0.25%	1.48%±0.34%	<0.001
APT_{Wmean}	2.76%±0.71%	2.94%±0.67%	0.221	1.23%±0.23%	1.71%±0.34%	<0.001
$rAPTw_{max}$	2.51%±0.79%	2.67%±0.73%	0.305	1.09%±0.22%	1.43%±0.31%	<0.001
$rAPTw_{min}$	2.03%±0.71%	2.10%±0.58%	0.578	0.51%±0.29%	0.95%±0.30%	<0.001
$rAPTw_{mean}$	2.28%±0.76%	2.40%±0.65%	0.448	0.76%±0.27%	1.17%±0.32%	<0.001

Abbreviations: (r)$APTW_{max}$, (relative) amide proton transfer-weighted max; (r)$APTW_{min}$, (relative) amide proton transfer-weighted min; (r)$APTW_{mean}$, (relative) amide proton transfer-weighted mean; SBM, solitary brain metastasis; GBM, glioblastoma.

Table 2

ROC analysis results of APTw parameter values in the peritumoral edema.

Parameter	AUC	95% CI	*P-value*	Cut-off	Sensitivity	Specificity	Accuracy
APT_{Wmax}	0.856	0.764–0.921	*P*<0.001	1.85%	93.3%	69.8%	79.5%
APT_{Wmin}	0.905	0.824–0.957	*P*<0.001	1.21%	84.4%	86.1%	85.2%
APT_{Wmean}	0.868	0.779–0.931	*P*<0.001	1.46%	86.7%	81.4%	81.8%
$rAPT_{Wmax}$	0.829	0.734–0.901	*P*<0.001	1.27%	80.0%	76.7%	76.1%
$rAPT_{Wmin}$	0.864	0.774–0.927	*P*<0.001	0.71%	77.8%	85.5%	79.5%
$rAPT_{Wmean}$	0.841	0.748–0.911	*P*<0.001	1.09%	82.2%	74.4%	77..3%

Abbreviations: (r)$APTW_{max}$, (relative)amide proton transfer-weighted max; (r)$APTW_{min}$, (relative)amide proton transfer-weighted min; (r)$APTW_{mean}$, (relative)amide proton transfer-weighted mean